



Cite this: DOI: 10.1039/c6tc05630j

## Bipolar hosts and non-doped deep-blue emitters (CIE<sub>y</sub> = 0.04) based on phenylcarbazole and 2-(2-phenyl-2H-1,2,4-triazol-3-yl)pyridine groups†

Huixia Xu,<sup>ab</sup> Peng Sun,<sup>ab</sup> Kexiang Wang,<sup>ab</sup> Jie Li,<sup>ab</sup> Fang Wang,<sup>ab</sup> Yanqin Miao,<sup>ab</sup> Hua Wang,<sup>ab</sup> Bingshe Xu<sup>ab</sup> and Wai-Yeung Wong<sup>ac</sup>

We have designed and synthesized four bipolar materials, **TAZ-1Cz**, **TAZ-2Cz**, **TAZ-3Cz** and **TAZ-4Cz**, using 2-(2-phenyl-2H-1,2,4-triazol-3-yl)pyridine (TAZ) as an electron-withdrawing group and phenylcarbazole as an electron-donating group. Their rigid molecular structures improve their thermal stability with high glass transition temperatures: 99 °C for **TAZ-2Cz**, 100 °C for **TAZ-3Cz** and 103 °C for **TAZ-4Cz**. Employing **TAZ-1Cz**, **TAZ-2Cz**, **TAZ-3Cz** and **TAZ-4Cz** as hosts, green phosphorescent organic light-emitting devices (PhOLEDs) with *fac*-tris(2-phenylpyridine)iridium as an emitter display maximum external quantum efficiencies (EQEs) of 15.8, 15.5, 16.0 and 13.0%, respectively. And blue PhOLEDs hosted by **TAZ-1Cz**, **TAZ-2Cz** and **TAZ-3Cz** achieved maximum current efficiencies of 8.6, 11.0 and 10.6 cd A<sup>-1</sup>, respectively. Furthermore, non-doped OLEDs using **TAZ-1Cz** and **TAZ-4Cz** as emitters exhibit electroluminescence (EL) peaks at 400 and 412 nm with CIE coordinates of (0.16, 0.04) and (0.15, 0.04), which are located in the deep-blue region.

Received 28th December 2016,  
Accepted 30th March 2017

DOI: 10.1039/c6tc05630j

rsc.li/materials-c

## Introduction

Phosphorescent organic light-emitting devices (PhOLEDs), which can reach theoretically 100% internal quantum efficiency, have attracted great attention.<sup>1</sup> In PhOLEDs, phosphorescent hosts play a key role in achieving efficient energy transfer from the hosts to emitters.<sup>2</sup> Many organic molecules can be used as hosts for green and red PhOLEDs,<sup>3</sup> while hosts for blue PhOLEDs are very rare due to the intrinsically high triplet level ( $E_T$ ) of blue emitters.<sup>4</sup>

Recently, bipolar non-doped blue-emitting materials (CIE<sub>y</sub> ≤ 0.10) based on organic molecules with balanced carrier-transport properties have drawn much attention due to their facile synthesis and low cost.<sup>5</sup> However, these blue fluorescent materials are not suitable for use as hosts for green or blue PhOLEDs because of

the low  $E_T$  (≤ 2.62 eV), while hosts for blue PhOLEDs with high  $E_T$ , whose emissions are located in the ultraviolet region, are also not suitable for use as blue fluorescent materials in non-doped OLEDs.<sup>6</sup>

Aimed at developing efficient bipolar hosts for green and blue PhOLEDs, and using them as non-doped deep-blue fluorescent emitters, we designed and synthesized four 2-(2-phenyl-2H-1,2,4-triazol-3-yl)pyridine (TAZ)- and carbazole (Cz)-based bipolar materials – **TAZ-1Cz**, **TAZ-2Cz**, **TAZ-3Cz** and **TAZ-4Cz**. Carbazole derivatives are widely utilized as donors in host materials due to their high  $E_T$  to prevent the back-energy transfer from the emitter to the host and sufficient hole-transport properties.<sup>7</sup> Meanwhile, 1,2,4-triazole has been used as an acceptor in bipolar hosts and ancillary ligands in metal complexes because of its excellent electron-transport characteristic.<sup>8</sup> Our previous report demonstrated that 9-(6-(3-phenyl-5-(pyridin-2-yl)-4H-1,2,4-triazol-4-yl)hexyl)-9H-carbazole (**PPHCz**) exhibited ultraviolet emission and a good bipolar ability.<sup>8b</sup> To shift the emission to the deep-blue region, the alkyl bridge between donors and acceptors was replaced by conjugated phenyl groups in this paper. By attaching a carbazole moiety to the different positions of the 2-(2-phenyl-2H-1,2,4-triazol-3-yl)pyridine skeleton, the four novel bipolar materials were synthesized (Fig. 1). In **TAZ-1Cz** and **TAZ-2Cz** compounds, carbazoles are linked by the *N*-phenyl, while the carbazoles are connected through C3- and C2-phenyl in **TAZ-3Cz** and **TAZ-4Cz**, respectively. To reach high  $E_T$ , the conjugation between the acceptor and the donor was broken in **TAZ-1Cz** and **TAZ-2Cz**.

<sup>a</sup> Key Laboratory of Interface Science and Engineering in Advanced Materials, Ministry of Education, Taiyuan University of Technology, Taiyuan, Shanxi 030024, P. R. China. E-mail: xuhuixia@tyut.edu.cn

<sup>b</sup> Shanxi Research Centre of Advanced Materials Science and Technology, Taiyuan, Shanxi, 030024, P. R. China

<sup>c</sup> Department of Applied Biology and Chemical Technology, The Hong Kong Polytechnic University, Hung Hom, Hong Kong, P. R. China

† Electronic supplementary information (ESI) available: Synthetic routes, absorption spectra in different solvents, phosphorescence spectra, electrochemical curves, electroluminescence performances of blue and red PhOLEDs, EQE versus luminance curves of green and red PhOLEDs hosted by CBP and electroluminescence spectra of non-doped OLEDs. See DOI: 10.1039/c6tc05630j

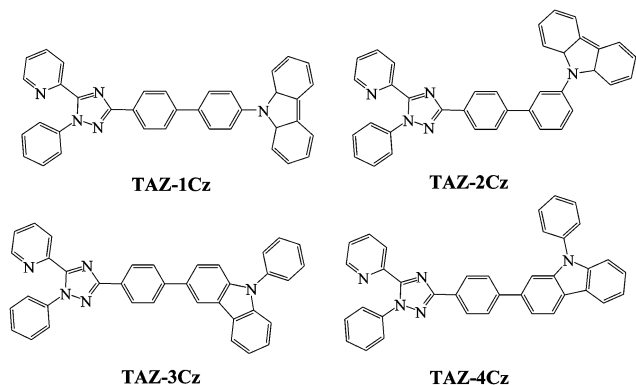


Fig. 1 Chemical structures of TAZ-1Cz, TAZ-2Cz, TAZ-3Cz and TAZ-4Cz.

The four bipolar materials possess twisted and rigid molecular structures, which result in deep-blue emissions, good thermal stabilities and carrier-transport abilities. They have not only been employed as emitters in fabricating non-doped deep-blue OLEDs, but have also been used as hosts to construct green and blue PhOLEDs. The green and blue PhOLEDs hosted by TAZ-2Cz exhibit maximum current efficiencies of 55.0 and 11.0 cd A<sup>-1</sup>. And the non-doped OLEDs using TAZ-4Cz as an emitter exhibit deep-blue emission with CIE coordinates of (0.15, 0.04).

## Results and discussion

The four bipolar materials were prepared by facile synthesis routes as shown in Scheme S1 (ESI<sup>†</sup>). Compound 2 was obtained by the Ullmann reaction between compound 1 and 1-iodobenzene, which was reacted with the corresponding donors to produce the bipolar materials by Suzuki coupling reactions. All of these materials exhibit good solubility in most common organic solvents. The molecular structures of the four bipolar materials were fully characterized by <sup>1</sup>H NMR, <sup>13</sup>C NMR, and elemental analyses.

Fig. 2 shows the TGA and DSC (inset) curves of the four bipolar materials and Table 1 summarizes the relevant data. The excellent thermal stabilities of the synthesized bipolar materials are manifested by their high decomposition temperatures ( $T_d$ : corresponding to 5% weight loss) in the range of 412–476 °C. Meanwhile, their glass transition temperatures ( $T_g$ ) are 99 °C for TAZ-2Cz, 100 °C

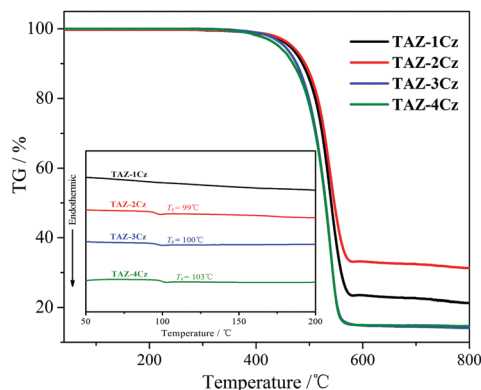


Fig. 2 TGA and DSC (inset) curves of all bipolar materials.

Table 1 Photophysical properties of all bipolar materials

Compound	$\lambda_{\text{abs}}^a$ (nm)	$\lambda_{\text{em}}^a$ (nm)	$E_g^b$ (eV)	HOMO/LUMO (eV)	$E_T^c$ (eV)	$T_d/T_g^d$ (°C)
TAZ-1Cz	290, 312	400	3.48	-5.71/-2.23	2.53	462/—
TAZ-2Cz	289, 342	402	3.64	-5.74/-2.10	2.62	467/99
TAZ-3Cz	259, 301	386	3.45	-5.63/-2.18	2.56	453/100
TAZ-4Cz	280, 315	400	3.42	-5.71/-2.29	2.51	442/103

<sup>a</sup> Measured in CH<sub>2</sub>Cl<sub>2</sub> solution of  $1 \times 10^{-5}$  M at room temperature.

<sup>b</sup> Calculated by the intersection of the UV-vis absorption and emission spectra. <sup>c</sup> Estimated from the highest vibronic peak phosphorescence spectra in 2-MeTHF at 77 K. <sup>d</sup> From TGA and DSC measurements.

for TAZ-3Cz and 103 °C for TAZ-4Cz, respectively. It is worth noting that no glass transition is detected in the DSC curve for TAZ-1Cz under the same conditions.

Much higher  $T_g$  values than those of commonly used host materials such as 1,3-bis(9H-carbazol-9-yl)benzene (mCP: 60 °C), 4,4'-N,N'-dicarbazolebiphenyl (CBP: 62 °C)<sup>9</sup> and some diphenylphosphine oxide derivatives<sup>10</sup> are observed, indicating that the introduction of the rigid TAZ moiety increases their morphological stability greatly.

Fig. 3 shows the UV-vis absorption and emission spectra of the synthesized bipolar materials in dichloromethane (CH<sub>2</sub>Cl<sub>2</sub>) solution at room temperature. Although the  $\pi$ - $\pi^*$  transition absorption character of donor and acceptor moieties is similar in the range of 260–300 nm for all four materials, the long-wavelength absorption bands are completely different. The absorption spectra of TAZ-1Cz with a shoulder peak at 312 nm and the absorption peak of TAZ-2Cz at 342 nm are attributed to the intramolecular charge-transfer (ICT) transitions from the donor to acceptor. The absorption spectrum of TAZ-3Cz displays a very weak ICT peak at 326 nm. Interestingly, ICT transition peaks in TAZ-4Cz may be covered due to the strong and broadened  $\pi$ - $\pi^*$  absorption at 315 nm. The emission peaks of all bipolar materials in this paper are located at 395–400 nm in CH<sub>2</sub>Cl<sub>2</sub> solution. According to the intersection of the absorption and emission bands in CH<sub>2</sub>Cl<sub>2</sub> solution, the energy gaps ( $E_g$ ) are estimated to be 3.48, 3.64, 3.45 and 3.42 eV for TAZ-1Cz, TAZ-2Cz, TAZ-3Cz and TAZ-4Cz, respectively (Table 1).

To better understand the photophysical properties of the four compounds, the UV-vis and PL spectra in solvents with different polarities were measured. The UV-vis absorption spectra seldom

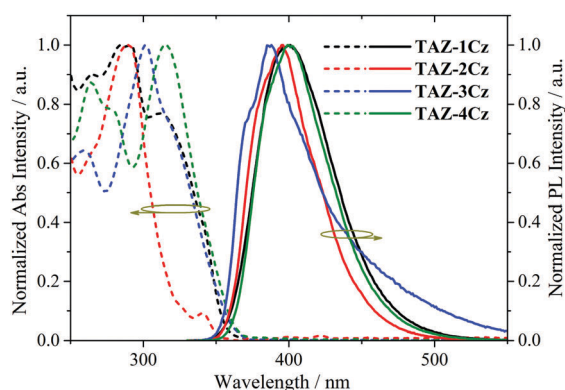


Fig. 3 Normalized UV-vis and PL spectra in CH<sub>2</sub>Cl<sub>2</sub> solution.

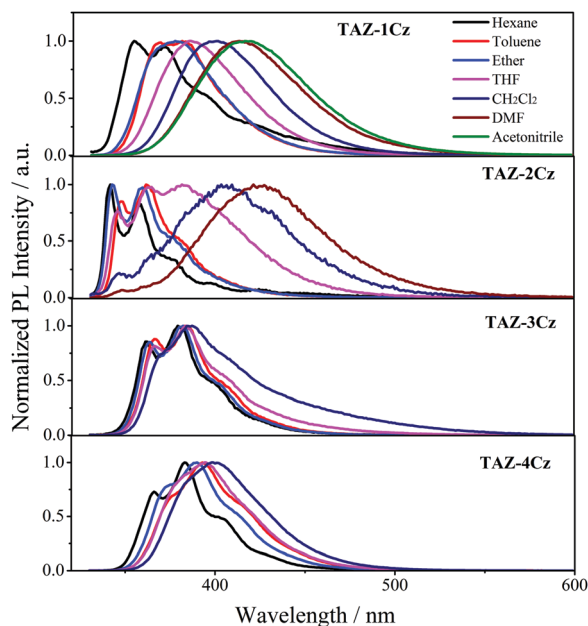


Fig. 4 PL spectra of **TAZ-1Cz**, **TAZ-2Cz**, **TAZ-3Cz** and **TAZ-4Cz** in different solvents at room temperature.

change in terms of shape and position in various solvents (Fig. S1, ESI<sup>†</sup>), implying a rather small dipolar change in the ground state in different solvents and the electronic structures of ground states are independent of the solvent polarity.

In contrast, the four bipolar materials exhibit distinct solvatochromic effects for the emission spectra as the solvent polarity increases due to the different conjugation of the molecules (Fig. 4). For **TAZ-1Cz** and **TAZ-2Cz** with carbazole N-linked to the phenyl moieties, significant bathochromic shifts are observed from 354/372 to 417 nm and 326/370 to 430 nm from low-polarity hexane to high-polarity acetonitrile.

Besides, the vibronic fine structures of emission spectra gradually disappear, and broad emission spectra emerge with the increase of the solvent polarity. These changes are consistent with the change in the excited state from the locally excited (LE) state to a strong charge-transfer (CT) excited state.<sup>11</sup> For **TAZ-3Cz** and **TAZ-4Cz** with the C3- and C2-positions of carbazole linked to the phenyl moieties, the PL behaviors were totally different. For **TAZ-3Cz**, the vibrational structures with emission peaks at 362 and 380 nm remain almost unchanged with the increase of the solvent polarity, suggesting that the locally excited state remains due to the full conjugation. In the case of **TAZ-4Cz**, the LE-to-CT state conversion is observed in the emission spectra in solvents from non-polar hexane to high-polarity *N,N*-dimethylformamide (DMF). However, the bathochromic shift value (from 367/384 to 400 nm) is much smaller than that of **TAZ-1Cz** and **TAZ-2Cz**, which could be ascribed to the limited conjugation of the molecules with the acceptor linked on the 2-position of the carbazole.

The low-temperature phosphorescence spectra of all bipolar materials, which were measured in 2-methyltetrahydrofuran (2-MeTHF) matrices at 77 K, showed fine vibronic structures, as seen in Fig. S2 (ESI<sup>†</sup>).  $E_T$ s are estimated to be 2.53, 2.62, 2.56

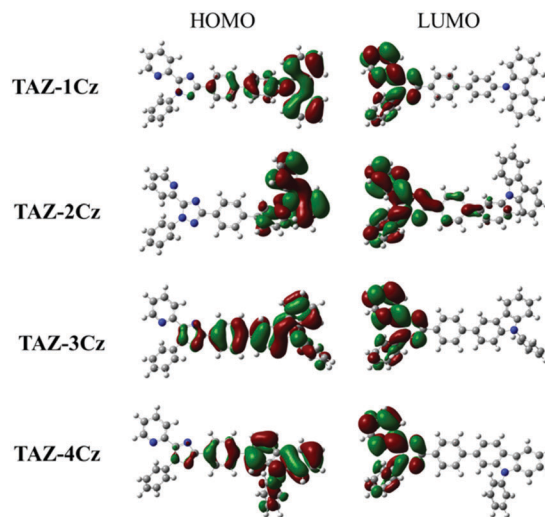


Fig. 5 HOMO and LUMO distributions for the four synthesized bipolar materials.

and 2.51 eV for **TAZ-1Cz**, **TAZ-2Cz**, **TAZ-3Cz** and **TAZ-4Cz**, respectively, according to the highest energy of the phosphorescence peaks. The highest  $E_T$  of compound **TAZ-2Cz** in all four bipolar materials is due to the broken conjugated structure with the N-linkage of carbazole. Remarkably, the  $E_T$  of **TAZ-2Cz** is higher than that of the blue emitter of iridium(III) bis[(4,6-difluorophenyl)pyridinato-*N,C*']picolinate (Firpic,  $E_T = 2.6$  eV), indicating that it can be used to fabricate blue PhOLEDs.<sup>12</sup>

The electrochemical behaviors were studied by cyclic voltammetry (CV). Because the oxidation process occurred in the carbazole unit, all four bipolar materials show similar oxidation curves (see Fig. S3, ESI<sup>†</sup>). The oxidation potentials of **TAZ-Cz**, **TAZ-2Cz**, **TAZ-3Cz** and **TAZ-4Cz** are 1.19, 1.20, 1.08 and 1.23 V, respectively. The corresponding  $E_{\text{HOMO}}/E_{\text{LUMO}}$  levels are estimated to be  $-5.71/-2.23$ ,  $-5.74/-2.10$ ,  $-5.63/-2.18$ , and  $-5.71/-2.29$  eV, respectively, by using the formulae  $E_{\text{HOMO}} = -4.8 - e(E_c^{\text{ox}} - E_f^{\text{ox}})V$  and  $E_{\text{LUMO}} = E_{\text{HOMO}} + E_g$  (HOMO: highest occupied molecular orbital; LUMO: lowest unoccupied molecular orbital). The linkage modes of carbazole and TAZ result in different electrochemical behaviors. To further study the electron structures of these bipolar materials, density functional theory (DFT) calculations were carried out at the B3LYP/6-31G(d) level. When the carbazole is linked through the *N*-phenyl and C3-phenyl in **TAZ-3Cz**, **TAZ-4Cz** and **TAZ-1Cz**, the HOMOs mainly disperse on the phenylcarbazole and partly on 1,2,4-triazole rings, in Fig. 5. When the carbazole is linked through the C2-phenyl in **TAZ-2Cz**, the HOMOs distribute on the phenylcarbazole. For all the compounds, the LUMOs mainly locate at the electron-deficient TAZ moieties. The completely separated distributions of the HOMOs and LUMOs and larger dihedral angle ( $56^\circ$ ) between the donor unit and nearby phenyl in **TAZ-2Cz** result in a higher  $E_T$  and low-lying  $E_{\text{HOMO}}$ . On the other hand, the smaller dihedral angle ( $37^\circ$ ) and better conjugation structure in **TAZ-3Cz** led to a high-lying  $E_{\text{HOMO}}$ . The calculated  $E_{\text{HOMO}}/E_{\text{LUMO}}$  levels are  $-5.35/-1.50$ ,  $-5.24/-1.39$ ,  $-5.13/-1.43$  and  $-5.31/-1.45$  eV for **TAZ-Cz**, **TAZ-2Cz**, **TAZ-3Cz** and **TAZ-4Cz**, respectively, which are in agreement with the experimental results (Table 1).

To investigate their bipolar charge-transport characteristics, we fabricated hole-only (HODs) and electron-only devices (EODs). The configurations of the HODs and EODs are ITO/MoO<sub>3</sub> (3 nm)/TCTA (10 nm)/bipolar materials (40 nm)/TCTA (10 nm)/Al (200 nm), and ITO/TPBi (10 nm)/bipolar materials (40 nm)/TPBi (10 nm)/LiF (1 nm)/Al (200 nm), respectively. Tris(4-carbazoyl-9-ylphenyl)amine (TCTA) in HODs and 1,3,5-tris(2-phenylbenzimidazolyl)-benzene (TPBi) in EODs were used to block the electron-injection from Al and the hole-injection from ITO. MoO<sub>3</sub> (molybdenum oxide) and LiF (lithium fluoride) serve as hole- and electron-injecting layers. The current density–voltage ( $J$ - $V$ ) curves of the HODs and EODs are shown in Fig. 6. The  $J$ - $V$  characteristics of the hole- and electron-only devices illustrate that all four compounds have bipolar charge-transport capacities as evidenced by the considerable hole/electron current density with similar magnitudes. The hole current density is slightly higher than that of electrons, which can be attributed to the high-lying LUMO energy level of the compound. The carrier-transport balance of TAZ-1Cz and TAZ-3Cz is superior to that of TAZ-2Cz and TAZ-4Cz.

To evaluate their electroluminescence (EL) properties, green phosphorescent OLEDs using *fac*-tris(2-phenylpyridine)iridium (Ir(ppy)<sub>3</sub>) ( $E_T = 2.4$  eV) as a dopant were fabricated with the following configuration: ITO/MoO<sub>3</sub> (3 nm)/NPB (30 nm)/TCTA (10 nm)/Host: Ir(ppy)<sub>3</sub> 8 wt% (20 nm)/TPBi (40 nm)/LiF (1 nm)/Al (200) (hosts: TAZ-1Cz for device G1, TAZ-2Cz for device G2, TAZ-3Cz for device G3 and TAZ-4Cz for device G4). The energy level diagrams of the devices and all molecular structures are shown in Fig. S4 (ESI<sup>†</sup>).

The current density–voltage–luminance ( $J$ - $V$ - $L$ ) characteristics, current density–efficiency and external quantum efficiency (EQE)–luminance curves for the green devices are shown in Fig. 7, and key device performance data are listed in Table 2. Fig. 7a shows the normalized EL spectra of these green devices. The EL spectra of devices G1–G4 are similar to the phosphorescent emitter Ir(ppy)<sub>3</sub>, indicating that the emission originates from the Ir(ppy)<sub>3</sub> dopant. Therefore, the triplet energy transfers from the host to the dopant are complete. In addition, the EL spectra of all devices remain quite stable under different voltages.

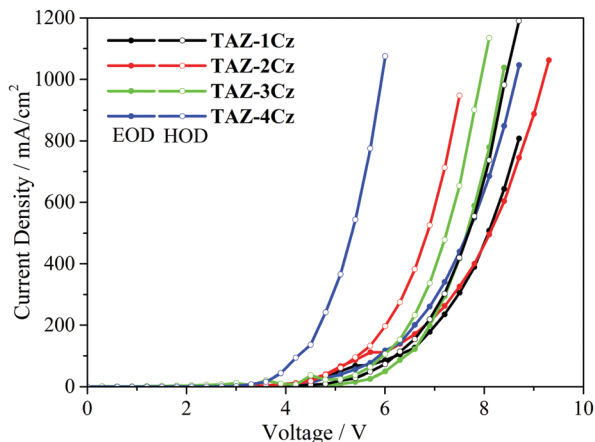


Fig. 6  $J$ - $V$  characteristics of electron-only and hole-only devices.

Devices G1, G3 and G4 show close turn-on voltage values ( $V_{on}$ , voltage at  $1.0 \text{ cd m}^{-2}$ ) of 3.3, 3.2 and 3.3 V. The highest  $V_{on}$  of 3.6 V in device G2 may be due to the large barrier to electron injection from TPBi to the host of TAZ-2Cz (the energy difference is 0.6 V between TPBi and TAZ-2Cz). Device G1 hosted by TAZ-1Cz exhibits a maximum current efficiency ( $\eta_{c,max}$ ) of  $55.0 \text{ cd A}^{-1}$ , a maximum power efficiency ( $\eta_{p,max}$ ) of  $41.3 \text{ lm W}^{-1}$  and a maximum external quantum efficiency (EQE<sub>max</sub>) of 15.5%. And device G2 hosted by TAZ-2Cz shows a performance with  $\eta_{c,max}$  of  $53.0 \text{ cd A}^{-1}$ ,  $\eta_{p,max}$  of  $40.0 \text{ lm W}^{-1}$  and EQE<sub>max</sub> of 16.0%. In comparison, when TAZ units are linked to the C3- and C2-phenyl of carbazole in TAZ-3Cz and TAZ-4Cz, their hosted devices G3 and G4 show inferior performance with maximum efficiencies of  $47.8 \text{ cd A}^{-1}$ ,  $35.1 \text{ lm W}^{-1}$ , and 13.9% for device G3 and  $46.1 \text{ cd A}^{-1}$ ,  $35.3 \text{ lm W}^{-1}$ , and 13.0% for device G4. The much better EL performance of device G2 than that of the other devices can be ascribed to high  $E_T$  and large  $E_g$ . Furthermore, it is found that devices G1, G2, G3 and G4 show EQEs of 12.4, 10.9, 11.8 and 4.8% at a luminance of  $1000 \text{ cd m}^{-2}$ , respectively. The percentage drops in EQE at a given field ( $F$ ) and luminance ( $L$ ) with reference to EQE<sub>max</sub> were calculated to be 20, 31.8, 15 and 63% using the equation  $\text{EQE}_{\text{roll-off}} = \frac{\text{EQE}_{\text{max}} - \text{EQE}(F,L)}{\text{EQE}_{\text{max}}} \times 100\%$  at a luminance of  $1000 \text{ cd m}^{-2}$ . The most balanced charge-transporting character of host TAZ-3Cz results in the lowest EQE<sub>roll-off</sub> and the maximum luminance ( $L_{max}$ ) ( $68\,330 \text{ cd m}^{-2}$ ) of device G3 in all devices.

Considering the high  $E_T$  and performances in the green devices of TAZ-1Cz, TAZ-2Cz and TAZ-3Cz, the blue and red PhOLEDs using Firpic ( $E_T = 2.6$  eV) and bis(1-phenyl-isoquinoline)(acetylacetonato)iridium(III) (Ir(piq)<sub>2</sub>acac,  $E_T = 2.25$  eV) as dopants were prepared with the structures of ITO/MoO<sub>3</sub> (3 nm)/NPB (30 nm)/TCTA (10 nm)/hosts:Firpic 15 wt% (20 nm)/TPBi (40 nm)/LiF (1 nm)/Al (100 nm) (host: TAZ-1Cz for device B1, TAZ-2Cz for device B2 and TAZ-3Cz for device B3) and ITO/MoO<sub>3</sub> (3 nm)/NPB (30 nm)/TCTA (10 nm)/hosts:Ir(piq)<sub>2</sub>acac 4 wt% (20 nm)/TPBi (50 nm)/LiF (1 nm)/Al (100 nm) (host: TAZ-1Cz for device R1, TAZ-2Cz for device R2, TAZ-3Cz for device R3 and TAZ-4Cz for device R4). The key data are also listed in Table 2 and the performances are displayed in Fig. S5 and S6 (ESI<sup>†</sup>). The EL spectra of blue PhOLEDs are consistent with the PL spectra of Firpic in Fig. S5a (ESI<sup>†</sup>), suggesting that a complete energy transfer from the host to Firpic can be achieved. Similarly, the TAZ-2Cz hosted device B2 exhibits the best performances with maximum  $L_{max}$ ,  $\eta_c$ ,  $\eta_p$  and EQE values of  $5412 \text{ cd m}^{-2}$ ,  $11.0 \text{ cd A}^{-1}$ ,  $7.3 \text{ lm W}^{-1}$  and 5.0%, respectively. The EL peaks of red PhOLEDs are located at 624 nm with shoulders at about 670 nm. Device R1 hosted by TAZ-1Cz shows better performance with maximum  $L_{max}$ ,  $\eta_c$ ,  $\eta_p$  and EQE values of  $27\,670 \text{ cd m}^{-2}$ ,  $12.1 \text{ cd A}^{-1}$ ,  $9.1 \text{ lm W}^{-1}$  and 16.2%, respectively. Furthermore, the luminescence efficiencies of all red PhOLEDs are superior to that of the device using CBP as a host (Fig. S7, ESI<sup>†</sup>).

Because the emissions of TAZ-1Cz and TAZ-4Cz with excellent carrier-transport properties are located in the deep-blue region, we fabricated non-doped devices with the following structures:

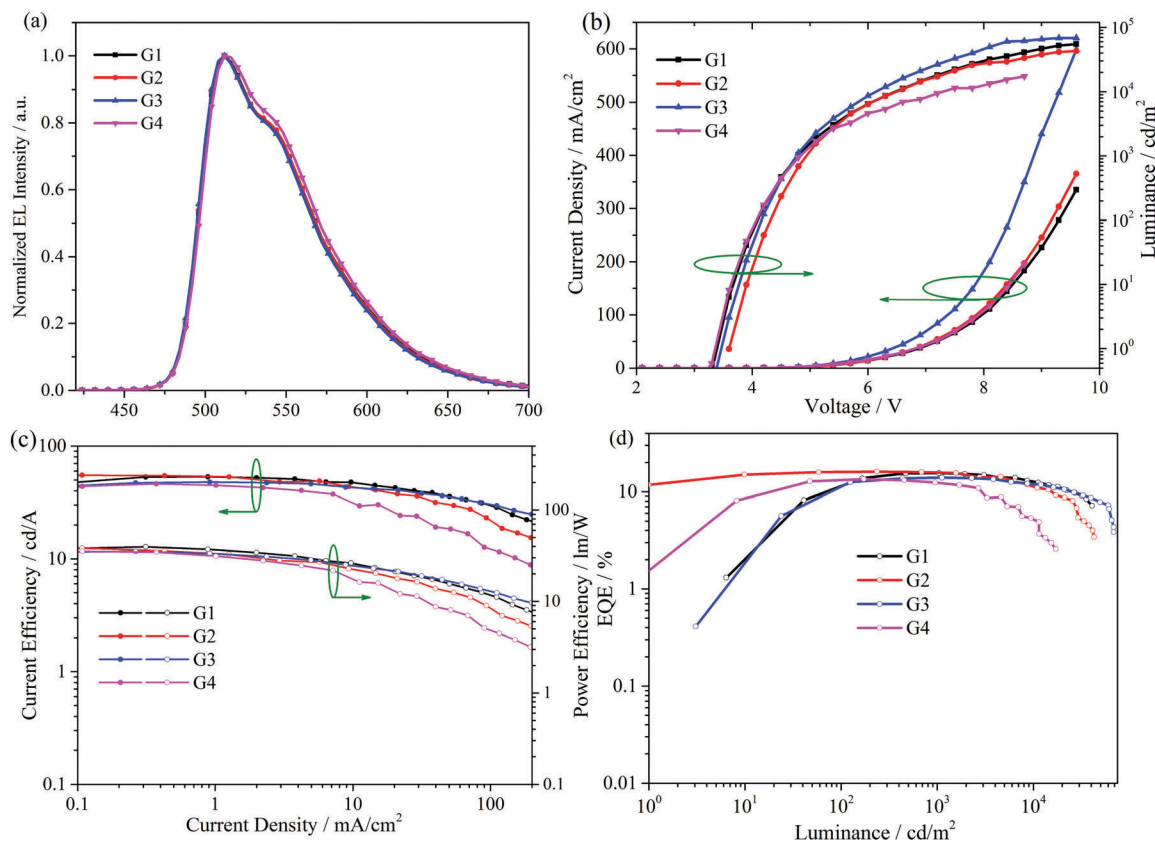


Fig. 7 (a) EL spectra, (b)  $J$ - $V$ - $L$  characteristics, (c) current efficiency-current density-power efficiency curves ( $\eta_c$ - $J$ - $\eta_p$ ) and (d) external quantum efficiency (EQE) versus luminance for green devices G1-G4.

Table 2 Device performances in this work

Device	Host	$\lambda_{\max}$ (nm)	CIE <sup>a</sup> (x, y)	$V_{\text{on}}$ (V)	$L_{\max}$ (cd m <sup>-2</sup> )	$\eta_c^b$ (cd A <sup>-1</sup> )	$\eta_p^c$ (lm W <sup>-1</sup> )	EQE <sub>max</sub> (%)
R1	TAZ-1Cz	624, 670	(0.67, 0.32)	3.8	27 670	12.1	9.1	16.2
R2	TAZ-2Cz	628, 670	(0.67, 0.32)	4.1	8008	11.4	7.9	16.1
R3	TAZ-3Cz	624, 670	(0.67, 0.32)	3.5	21 590	11.9	9.1	16.3
R4	TAZ-4Cz	628, 670	(0.67, 0.32)	3.8	14 750	11.9	8.9	16.1
G1	TAZ-1Cz	512, 540	(0.31, 0.60)	3.3	55 170	53.2	40.0	15.5
G2	TAZ-2Cz	512, 540	(0.31, 0.59)	3.6	42 710	55.0	41.3	16.0
G3	TAZ-3Cz	512, 540	(0.30, 0.59)	3.2	68 330	47.8	35.2	13.9
G4	TAZ-4Cz	512, 540	(0.31, 0.60)	3.3	17 210	46.1	35.3	13.0
B1	TAZ-1Cz	476	(0.13, 0.34)	3.3	2922	8.6	7.0	3.8
B2	TAZ-2Cz	472	(0.16, 0.33)	3.9	5412	11.0	7.3	5.0
B3	TAZ-3Cz	476	(0.16, 0.34)	3.6	3664	10.6	8.6	4.8
DB1		400	(0.16, 0.04)	3.9	784	0.53	0.43	1.65
DB2		412	(0.16, 0.04)	3.9	1478	0.68	0.58	2.48

<sup>a</sup> The CIE coordination at a voltage of 8 V. <sup>b</sup> The maximum current efficiency. <sup>c</sup> The maximum power efficiency.

ITO/MoO<sub>3</sub> (3 nm)/NPB (30 nm)/TCTA (10 nm)/TAZ-1Cz or TAZ-4Cz (30 nm)/TPBI (35 nm)/LiF (1 nm)/Al (100 nm) (TAZ-1Cz for device DB1, TAZ-4Cz for device DB2). The EL spectra,  $J$ - $V$ - $L$  characteristics,  $\eta_c$ - $J$ - $\eta_p$  and EQE-luminance curves are shown in Fig. 8 and the corresponding EL data are also listed in Table 2. Both devices DB1 and DB2 exhibit deep-blue emission with CIE coordinates of (0.16, 0.04) and (0.15, 0.04). And their EL peaks are located at 400 and 412 nm, respectively. The CIE<sub>y</sub> values are smaller than the NTSC (National Television Standards Committee) blue standard (CIE<sub>y</sub> = 0.08). In addition,

the EL spectra remain almost unchanged under different driving voltages from 5 to 10 V (Fig. S8, ESI<sup>†</sup>). Device DB1 using TAZ-1Cz as an emitter exhibits a turn-on voltage of 3.9 V, maximum  $\eta_c$  of 0.53 cd A<sup>-1</sup>,  $\eta_p$  of 0.43 lm W<sup>-1</sup> and EQE of 1.65%, respectively. Device DB2 employing TAZ-4Cz as an emitter exhibits superior performance to that of device DB1 with a  $V_{\text{on}}$  of 3.9 V, maximum  $\eta_c$  of 0.68 cd A<sup>-1</sup>,  $\eta_p$  of 0.58 lm W<sup>-1</sup> and EQE of 2.48% due to its conjugation structure. It is worth noting that the EQE roll-offs for non-doped deep-blue devices are negligible, indicating a well-balanced charge-transport property.

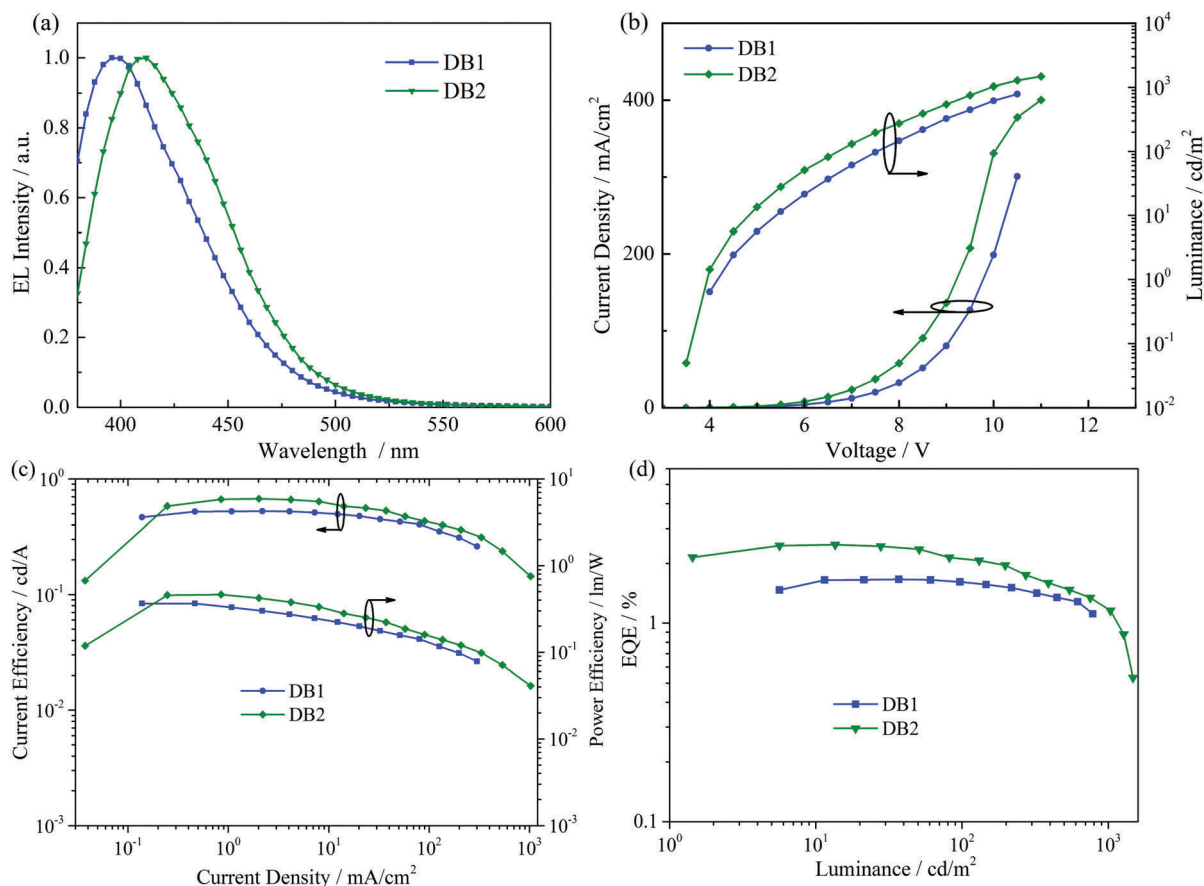


Fig. 8 (a) EL spectra, (b)  $J$ - $V$ - $L$  characteristics, (c)  $\eta_c$ - $J$ - $\eta_p$  and (d) external quantum efficiency (EQE) versus luminance curves of non-doped deep-blue devices.

## Conclusions

In summary, four bipolar materials **TAZ-1Cz**, **TAZ-2Cz**, **TAZ-3Cz** and **TAZ-4Cz**, using the 1,2,4-triazole derivative as an acceptor and carbazole as a donor, have not only been used as non-doped deep-blue fluorescent emitters in OLEDs, but also as host materials to fabricate blue, green and red PhOLEDs. The different linkage modes of donors and acceptors result in various photophysical properties. **TAZ-1Cz** and **TAZ-2Cz** with N-linked carbazole exhibit obvious conversion from LE to CT state transition. Compounds **TAZ-2Cz** and **TAZ-3Cz** possess higher  $E_{TS}$ s of 2.56 and 2.62 eV. PhOLEDs hosted by **TAZ-2Cz** show excellent performances among all devices with efficiencies of  $55.0 \text{ cd A}^{-1}$  and  $41.3 \text{ lm W}^{-1}$  and maximum EQE of 16% in green devices and  $11.0 \text{ cd A}^{-1}$ ,  $7.3 \text{ lm W}^{-1}$  and 5.0% in blue devices. The non-doped deep-blue device using **TAZ-4Cz** as an emitter exhibits a maximum EQE of 2.48%. Our results demonstrate that the bipolar host materials **TAZ-1Cz** and **TAZ-4Cz** may also be excellent deep-blue fluorescent emitters.

## Experimental

### Materials and measurements

$^1\text{H-NMR}$  and  $^{13}\text{C-NMR}$  spectra were measured on a Switzerland Bruker DRX600. C, H, and N microanalyses were carried out

with an Elemental Vario EL elemental analyzer. UV-vis absorption spectra were measured using a Lambda Bio 40. The photoluminescence (PL) spectra were recorded using a HORIBA FluoroMax-4 spectrophotometer. The low-temperature phosphorescence spectra at 77 K in 2-methyltetrahydrofuran (2-MeTHF) were recorded on an Edinburgh F-980 spectrometer. Thermogravimetric analysis (TGA) curves were obtained using a Netzsch TG 209F3 under a dry nitrogen atmosphere at a heating rate of  $10 \text{ }^\circ\text{C min}^{-1}$  from room temperature to  $800 \text{ }^\circ\text{C}$ . Differential scanning calorimetry (DSC) was performed on a DSC Q2000 at a heating rate of  $10 \text{ }^\circ\text{C min}^{-1}$  from 20 to  $300 \text{ }^\circ\text{C}$ , then cooling to room temperature rapidly, and heating to  $300 \text{ }^\circ\text{C}$  at a heating rate of  $10 \text{ }^\circ\text{C min}^{-1}$  again, from which the melting temperature ( $T_m$ ) was obtained from the first heating scan and the glass transition temperature ( $T_g$ ) was determined from the second heating scan.

Cyclic voltammetry (CV) was carried out in  $\text{CH}_2\text{Cl}_2$  solution with chromatographic purity at room temperature using a CHI 660E voltammetry analyzer. Tetrabutylammonium hexafluorophosphate (TBAPF6) (0.1 M) was used as a supporting electrolyte. A platinum wire was used as a working electrode. A platinum electrode is a counter and a calomel electrode is a reference with ferrocenium-ferrocene ( $\text{Fc}^+/\text{Fc}$ ) as an internal standard. The scan rate for CV curves is  $100 \text{ mV s}^{-1}$ . The highest occupied molecular orbital level ( $E_{\text{HOMO}}$ ) was calculated according to the equation

$E_{\text{HOMO}} = -4.8 - e(E_{\text{c}}^{\text{ox}} - E_{\text{f}}^{\text{ox}})$ , where  $E_{\text{c}}^{\text{ox}}$  is the first oxidation peaks measured from CV curves and  $E_{\text{f}}^{\text{ox}}$  is the oxidation peak of ferrocene. The lowest unoccupied molecular orbital level ( $E_{\text{LUMO}}$ ) was calculated from the equation  $E_{\text{LUMO}} = E_{\text{HOMO}} + E_{\text{g}}$ , and  $E_{\text{g}}$  is the intersection of the absorption and emission spectra.

Theoretical calculations were performed using the Gaussian 03 package. Geometry optimization was performed using density functional theory (DFT) in B3LYP/6-31G(d) basis sets. The molecular orbitals were visualized using GaussView 5.0.

### OLED fabrication and measurements

PhOLEDs and non-doped devices with an area of  $3 \times 3 \text{ mm}^2$  were fabricated by vacuum deposition onto an indium tin oxide (ITO) glass substrate. The ITO glass substrate was cleaned in order with deionized water, acetone and ethanol. The electroluminescence (EL) spectra and CIE coordinates were measured by a PR-655 spectrophotometer. The current density–voltage–luminance ( $J$ – $V$ – $L$ ) characteristics of PhOLEDs and OLEDs were recorded using a Keithley 2400 Source Meter and an ST-900M Spot Brightness Meter. The EQE values were calculated according to previously reported methods.<sup>11a</sup> All measurements were carried out at room temperature under ambient conditions.

### Synthesis

The starting reagents were purchased from commercial companies and used without further purification. Solvents for synthesis were purified according to standard procedures prior to use. All reactions were performed under nitrogen atmosphere. The synthetic routes of all host materials are presented in Scheme S1 (ESI†). And the synthesis of 2-(5-phenyl-4*H*-1,2,4-triazol-3-yl)pyridine (**1**) has been reported.<sup>13</sup>

**Synthesis of 2-(5-(4-bromophenyl)-2-phenyl-2*H*-1,2,4-triazol-3-yl)pyridine (**2**).** Compound **1** (2.28 g, 7.6 mmol), iodobenzene (2.45 g, 12 mmol), 1,10-phenanthroline (0.96 g, 4.8 mmol), copper(i) iodide (0.48 g, 2.5 mmol) and caesium carbonate (3.72 g, 11 mmol) were dissolved in DMF (40 mL). The mixture was stirred vigorously for 10 min at room temperature and subsequently refluxed under a nitrogen atmosphere for 24 h. After being cooled to RT, the mixture was poured into water (50 mL) and extracted with DCM (200 mL). The organic extracts were washed with water and dried over anhydrous  $\text{MgSO}_4$ . The product was then obtained by column chromatography on silica gel with petroleum ether/ethyl acetate (2 : 1) as an eluent to yield a white solid (yield: 75%).  $^1\text{H NMR}$  (600 MHz,  $\text{CDCl}_3$ ,  $\delta$ ): 8.53 (dd,  $J = 4.7, 1.4 \text{ Hz}$ , 1H), 8.18–8.10 (m, 2H), 7.91 (d,  $J = 7.9 \text{ Hz}$ , 1H), 7.81–7.76 (m, 1H), 7.63–7.58 (m, 2H), 7.44 (s, 5H), 7.32 (dd,  $J = 7.4, 4.9 \text{ Hz}$ , 1H).

**Synthesis of TAZ-1Cz.** Compound **2** (3.76 g, 10 mmol), 9-(4-(4,4,5,5-tetramethyl-1,3,2-dioxaborolan-2-yl)phenyl)-9*H*-carbazole (4.61 g, 12 mmol), tetrakis(triphenylphosphine)palladium(0) ( $\text{Pd}(\text{PPh}_3)_4$ ) (170 mg, 0.15 mmol), and sodium carbonate (3.18 g, 30 mmol) were dissolved in tetrahydrofuran (THF) (40 mL). The mixture was heated to reflux for 24 h under a nitrogen atmosphere. After being cooled to room temperature, the mixture was poured into water (50 mL) and extracted with  $\text{CH}_2\text{Cl}_2$  (200 mL). The organic extracts were washed with water and dried over anhydrous  $\text{MgSO}_4$ .

The product was then obtained by column chromatography on silica gel with petroleum ether/ethyl acetate (3 : 1) as an eluent to yield a white solid. Yield: 64%.  $^1\text{H NMR}$  (600 MHz,  $\text{CDCl}_3$ ,  $\delta$ ): 8.54 (dd,  $J = 4.7, 1.6 \text{ Hz}$ , 1H), 8.41–8.38 (m, 2H), 8.16 (dt,  $J = 7.8, 0.9 \text{ Hz}$ , 2H), 7.98 (dt,  $J = 7.9, 1.0 \text{ Hz}$ , 1H), 7.92–7.89 (m, 2H), 7.83–7.80 (m, 3H), 7.69–7.66 (m, 2H), 7.50–7.42 (m, 9H), 7.35–7.33 (m, 1H), 7.31 (ddd,  $J = 7.9, 7.0, 1.1 \text{ Hz}$ , 2H).  $^{13}\text{C NMR}$  (150 MHz,  $\text{CDCl}_3$ ,  $\delta$ ): 164.44, 156.39, 152.38, 150.52, 144.02, 143.78, 142.66, 141.81, 140.01, 139.64, 132.95, 131.86, 131.58, 131.38, 130.27, 130.19, 130.17, 128.91, 128.49, 127.36, 127.30, 126.39, 123.24, 122.92, 112.77. Anal. calcd for  $\text{C}_{37}\text{H}_{25}\text{N}_5$ : C, 82.37; H, 4.64; N, 12.99. Found: C, 82.44; H, 4.67; N, 12.78 (%).

**TAZ-2Cz, TAZ-3Cz and TAZ-4Cz** were prepared *via* similar procedures to compound **TAZ-1Cz**.

**TAZ-2Cz.** Yield: 71%.  $^1\text{H NMR}$  (600 MHz,  $\text{CDCl}_3$ ,  $\delta$ ): 8.54–8.52 (m, 1H), 8.37–8.34 (m, 2H), 8.17 (d,  $J = 7.7 \text{ Hz}$ , 2H), 7.95 (d,  $J = 7.8 \text{ Hz}$ , 1H), 7.88 (s, 1H), 7.81–7.76 (m, 4H), 7.70 (t,  $J = 7.8 \text{ Hz}$ , 1H), 7.57 (dt,  $J = 7.9, 1.4 \text{ Hz}$ , 1H), 7.50–7.41 (m, 9H), 7.34–7.29 (m, 3H).  $^{13}\text{C NMR}$  (150 MHz,  $\text{CDCl}_3$ ,  $\delta$ ): 164.35, 156.37, 152.38, 150.47, 145.53, 143.86, 143.85, 141.76, 141.22, 139.64, 133.24, 133.15, 131.86, 131.58, 130.21, 130.17, 129.05, 128.93, 128.63, 128.47, 127.37, 127.29, 126.34, 123.25, 122.89, 112.74. Anal. calcd for  $\text{C}_{37}\text{H}_{25}\text{N}_5$ : C, 82.37; H, 4.64; N, 12.99. Found: C, 82.94; H, 4.64; N, 12.97 (%).

**TAZ-3Cz.** Yield: 66%.  $^1\text{H NMR}$  (600 MHz,  $\text{CDCl}_3$ ,  $\delta$ ): 8.54 (d,  $J = 4.8 \text{ Hz}$ , 1H), 8.44 (dd,  $J = 1.9, 0.6 \text{ Hz}$ , 1H), 8.38–8.36 (m, 2H), 8.23 (dt,  $J = 7.7, 1.0 \text{ Hz}$ , 1H), 7.97 (d,  $J = 7.9 \text{ Hz}$ , 1H), 7.86–7.83 (m, 2H), 7.81 (td,  $J = 7.7, 1.8 \text{ Hz}$ , 1H), 7.74 (dd,  $J = 8.5, 1.8 \text{ Hz}$ , 1H), 7.66–7.58 (m, 4H), 7.51–7.42 (m, 9H), 7.33 (tdd,  $J = 7.9, 3.9, 2.4 \text{ Hz}$ , 2H).  $^{13}\text{C NMR}$  (150 MHz,  $\text{CDCl}_3$ ,  $\delta$ ): 164.70, 156.29, 152.34, 150.62, 145.83, 144.32, 143.47, 141.86, 140.59, 139.60, 135.82, 132.82, 131.82, 131.49, 130.44, 130.24, 130.04, 130.00, 129.06, 128.50, 128.31, 127.38, 127.22, 126.87, 126.43, 123.34, 123.03, 121.69, 112.96, 112.84. Anal. calcd for  $\text{C}_{37}\text{H}_{25}\text{N}_5$ : C, 82.37; H, 4.64; N, 12.99. Found: C, 81.16; H, 4.58; N, 12.72 (%).

**TAZ-4Cz.** Yield: 64%.  $^1\text{H NMR}$  (600 MHz,  $\text{CDCl}_3$ ,  $\delta$ ): 8.53 (ddd,  $J = 4.8, 1.8, 1.0 \text{ Hz}$ , 1H), 8.33–8.30 (m, 2H), 8.22–8.19 (m, 1H), 8.17 (dd,  $J = 7.7, 1.0 \text{ Hz}$ , 1H), 7.95 (dt,  $J = 7.8, 1.0 \text{ Hz}$ , 1H), 7.79 (td,  $J = 7.7, 1.8 \text{ Hz}$ , 1H), 7.77–7.74 (m, 2H), 7.66–7.60 (m, 6H), 7.50 (tt,  $J = 6.9, 1.8 \text{ Hz}$ , 1H), 7.48–7.40 (m, 7H), 7.33–7.29 (m, 2H).  $^{13}\text{C NMR}$  (150 MHz,  $\text{CDCl}_3$ ,  $\delta$ ): 164.58, 156.31, 152.35, 150.57, 145.80, 144.48, 144.44, 141.84, 141.82, 140.56, 139.60, 134.68, 132.92, 132.35, 131.82, 131.51, 131.14, 130.55, 130.54, 130.20, 129.96, 128.94, 128.49, 127.37, 127.23, 126.06, 125.76, 123.51, 123.28, 123.01, 122.53, 112.73, 111.06. Anal. calcd for  $\text{C}_{37}\text{H}_{25}\text{N}_5$ : C, 82.37; H, 4.64; N, 12.99. Found: C, 81.83; H, 4.59; N, 13.00 (%).

### Acknowledgements

This work was financially supported by the International Science and Technology Cooperation Program of China (2012DFR50460), the National Natural Scientific Foundation of China (21071108, 60976018, 61274056 and 61205179), the Natural Science Foundation of Shanxi Province (2015021070), the Program for Changjiang Scholar and Innovation Research Team in University (IRT0972),

and the Shanxi Provincial Key Innovative Research Team in Science and Technology (201513002-10).

## References

- (a) H. Uoyama, K. Goushi, K. Shizu, H. Nomura and C. Adachi, *Nature*, 2012, **492**, 234; (b) G. Xie, X. Li, D. Chen, Z. Wang, X. Cai, D. Chen, Y. Li, K. Liu, Y. Cao and S.-J. Su, *Adv. Mater.*, 2016, **28**, 181; (c) B. Wang, G. Mu, X. Lv, L. Ma, S. Zhuang and L. Wang, *Org. Electron.*, 2016, **34**, 179; (d) J. W. Sun, J. Y. Baek, K.-H. Kim, J.-S. Huh, S.-K. Kwon, Y.-H. Kim and J.-J. Kim, *J. Mater. Chem. C*, 2017, **5**, 1027; (e) P. Tao, W.-L. Li, J. Zhang, S. Guo, Q. Zhao, H. Wang, B. Wei, S.-J. Liu, X.-H. Zhou, Q. Yu, B.-S. Xu and W. Huang, *Adv. Funct. Mater.*, 2016, **26**, 881.
- (a) C. Yao, Z. Xue, M. Lian, X. Xu, J. Zhao and G. Zhou, *J. Organomet. Chem.*, 2015, **784**, 31; (b) Y. Wu, D. Yu, W.-Y. Wong, B. Liu, J. Zhao, C. Luo, F. Lu, S. Tao and Q. Tong, *J. Mater. Chem. C*, 2016, **4**, 2003; (c) M. Zhu, Y. Li, J. Miao, B. Jiang, C. Yang, H. Wu, J. Qin and Y. Cao, *Org. Electron.*, 2014, **15**, 1598.
- (a) Y. Nagai, H. Sasabe, S. Ohisa and J. Kido, *J. Mater. Chem. C*, 2016, **4**, 9476; (b) J. Zhao, Y. Yu, X. Yang, X. Yan, H. Zhang, X. Xu, G. Zhou, X. Ran and W.-Y. Wong, *ACS Appl. Mater. Interfaces*, 2015, **7**(44), 24703; (c) S. K. Jeon, C. S. Oh, M. Kim, K. S. Yooka and J. Y. Lee, *J. Mater. Chem. C*, 2016, **4**, 1606; (d) Y. Chen, W. Liang, W. H. Choi, J. Huang, Q. Dong, F. Zhu and J. Su, *Dyes Pigm.*, 2015, **123**, 196; (e) L. Duan, J. Qiao, Y. Sun and Y. Qiu, *Adv. Mater.*, 2011, **23**, 1137.
- (a) Y. Zhao, C. Wu, P. Qiu, X. Li, Q. Wang, J. Chen and D. Ma, *ACS Appl. Mater. Interfaces*, 2016, **8**, 2635; (b) K. S. Yook and J. Y. Lee, *Chem. Rec.*, 2016, **16**, 159; (c) S. M. Kim, J. H. Kim, S. K. Jeon and J. Y. Lee, *Dyes Pigm.*, 2016, **125**, 274; (d) H. Li, R. Bi, T. Chen, K. Yuan, R. Chen, Y. Tao, H. Zhang, C. Zheng and W. Huang, *ACS Appl. Mater. Interfaces*, 2016, **8**, 7274.
- (a) H. Liu, Q. Bai, W. Li, Y. Guo, L. Yao, Y. Gao, J. Li, P. Lu, B. Yang and Y. Ma, *RSC Adv.*, 2016, **6**, 70085; (b) W.-C. Chen, C.-S. Lee and Q.-X. Tong, *J. Mater. Chem. C*, 2015, **3**, 10957; (c) W. Li, D. Liu, F. Shen, D. Ma, Z. Wang, T. Feng, Y. Xu, B. Yang and Y. Ma, *Adv. Funct. Mater.*, 2012, **22**, 2797; (d) J. Jayabharathi, A. Prabhakaran, V. Thanikachalam and M. Sundharesan, *RSC Adv.*, 2016, **6**, 62208.
- (a) Q. Zhang, J. Li, K. Shizu, S. Huang, S. Hirata, H. Miyazaki and C. Adachi, *J. Am. Chem. Soc.*, 2012, **134**, 14706; (b) Y.-M. Xie, L.-S. Cui, F.-S. Zu, F. Igbari, M.-M. Xue, Z.-Q. Jiang and L.-S. Liao, *Org. Electron.*, 2015, **26**, 25; (c) Y.-K. Wang, Y.-L. Deng, X.-Y. Liu, X.-D. Yuan, Z.-Q. Jiang and L.-S. Liao, *Dyes Pigm.*, 2015, **122**, 6.
- (a) L. Wang, W.-Y. Wong, M.-F. Lin, W.-K. Wong, K.-W. Cheah, H.-L. Tam and C. H. Chen, *J. Mater. Chem.*, 2008, **18**, 4529; (b) C. S. Oh, J. Y. Lee, C. H. Noh and S. H. Kim, *J. Mater. Chem. C*, 2016, **4**, 3792; (c) X. Lv, B. Wang, B. Pan, Z. Huang, S. Xiang, J. Tan, W. Yi, H. Huang and L. Wang, *RSC Adv.*, 2016, **6**, 46775; (d) W. C. Lin, H. W. Lin, E. Mondal and K. T. Wong, *Org. Electron.*, 2015, **17**, 1.
- (a) S. Y. Lee, T. Yasuda, H. Nomura and C. Adachi, *Appl. Phys. Lett.*, 2012, **101**, 093306; (b) H. Xu, P. Sun, K. Wang, Y. Miao, T. Yang, H. Wang, B. Xu and W.-Y. Wong, *Tetrahedron*, 2016, **72**, 4408; (c) C. Adachi, *Jpn. J. Appl. Phys.*, 2014, **53**, 060101; (d) D. Liu, D. Li, M. Wang and W. Li, *J. Mater. Chem. C*, 2016, **4**, 7260.
- A. Wada, T. Yasuda, Q. Zhang, Y. S. Yang, I. Takasu, S. Enomoto and C. Adachi, *J. Mater. Chem. C*, 2013, **1**, 2404.
- M.-H. Tsai, Y.-H. Hong, C.-H. Chang, H.-C. Su, C.-C. Wu, A. Matoliukstyte, J. Simokaitiene, S. Grigalevicius, J. V. Grazulevicius and C.-P. Hsu, *Adv. Mater.*, 2007, **19**, 862.
- (a) H. Liu, Q. Bai, L. Yao, H. Zhang, H. Xu, S. Zhang, W. Li, Y. Gao, J. Li, P. Lu, H. Wang, B. Yang and Y. Ma, *Chem. Sci.*, 2015, **6**, 3797; (b) Y. Gao, S. Zhang, Y. Pan, L. Yao, H. Liu, Y. Guo, Q. Gu, B. Yang and Y. Ma, *Phys. Chem. Chem. Phys.*, 2016, **18**, 24176; (c) X. Tang, Q. Bai, Q. Peng, Y. Gao, J. Li, Y. Liu, L. Yao, P. Lu, B. Yang and Y. Ma, *Chem. Mater.*, 2015, **27**, 7050; (d) H. Liu, Q. Bai, W. Li, Y. Guo, L. Yao, Y. Gao, J. Li, P. Lu, B. Yang and Y. Ma, *RSC Adv.*, 2016, **6**, 70085; (e) X. Ouyang, X. Zhang and Z. Ge, *Dyes Pigm.*, 2014, **103**, 39.
- K. S. Yook and J. Y. Lee, *Chem. Rec.*, 2016, **16**, 159.
- H. Xu, Y. Yue, L. Qu, Y. Hao, H. Wang, L. Chen and B. Xu, *Dyes Pigm.*, 2013, **99**, 67.